Exp. Theo. NANOTECHNOLOGY 3 (2019) 197-212 https://doi.org/10.56053/3.2.197

Structural and optical analysis of chalcogenide nanostructures

S. Chernkov[1,*], *P. Badov*[2]

[1]National University of Science and Technology MISiS, 119049, Moscow, Leninsky Prospekt, 4, Russia
2Physics Department, University of Chemical Technology and Metallurgy, Sofia, Bulgaria
[*]) Email: schernkov@misis.ru

Received 15/01/2019, *Accepted* 15/04/2019, *Published* 15/5/2019

Ultra-thin crystalline films of Bi-based chalcogenides were deposited with the aid of vacuum thermal evaporation technique. The influence of thermal annealing on the optical properties of Bi2Te3-Bi2Se3 films with different thicknesses has been investigate. Optical transmittance and reflectance of the as prepared and annealed films were measured in the wavelength range 290–2700 nm using a double beam spectrophotometer. Fundamental optical properties such as absorption coefficient and energy bend gap were derived based on the measured spectra and film's thickness. We demonstrate in the present work that the synergy of annealing and thickness reduction can be exploited for light transmittance enhancements, and consequently optoelectronic applications including transparent electrode can be achieved.

Keywords: Thin films; Chalcogenides; Optical transmission; Band gap.

1. INTRODUCTION

Considerable attention was given to Bi_2Te_3 over the past years, due to its high thermoelectric properties, however, the attention was mainly devoted to Bi_2Te_3 on its bulk form that is why, and no much work was carried out on thin Bi_2Te_3 films. In addition, very few measurements of the optical properties were reported [1]. J. Dheepa et al. [2] have studied the optical properties of thin Bi_2Te_3 films prepared by thermal evaporated and showed that the films are hexagonal and polycrystalline in structure.

Although annealing processes are known to enhance the transport properties [3], a few number of reports discussing the structural features changing by the effect of annealing and their relation with transport properties on the Bi_2Te_3 thin films.

Practically, Bi_2Te_3 compound is usually obtained with directional solidification from melt or powder metallurgy processes. As one of the V_2VI_3 binary chalcogenide compound semiconductors it has very interesting applications in optoelectronic and electrochemical devices such as heat pumps infrared sensors and high efficiency photovoltaic solar cells [4-8].

Bi_2Te_3 is exactly like Bi_2Se_3, possesses stacked layers showing laminated structure that are held together by weak van der Waals interactions. Layers exhibit quintuple structure in which five atoms are covalently bonded together along the z axis in the order of Te-Bi-Te-Bi-Te. Owing to that, it is possible to exfoliate bulk Bi_2Te_3 into few-layer nanosheets due to the weak interaction between layers. Few-layer Bi_2Te_3 is recently considered as a highly promising and excellent material.

The purpose of the present work is to report experimental results of the preparation of thin Bi_2Te_3-Bi_2Se_3 films by vacuum thermal evaporation technique and to study optical properties of the prepared films of at different thicknesses after and before annealing treatment. In addition, the effect of annealing process on the structure and optical properties is studied as well.

2. EXPERIMENTAL DETAILS

Thin crystalline of $Bi_2 (Te_{1-x}Se_x)_3$ films were deposited onto optically flat glass substrates, BK7 type; deposition process was carried out by thermal evaporation technique at high vacuum. Substrates were kept at room temperature during the evaporation process and were rotated to obtain uniform layers. Thickness measurements were controlled by thickness monitor, moreover; thickness was measured with the aid of micro interferometer optical microscope (MODEL MUU10) as well. Different thicknesses were made for purpose of studying the thickness reduction effect. Ultra-thin layers were prepared at thickness range between 100 nm and down to 15 nm. Annealing process was conducted for all thicknesses under the study at different temperatures for 3h. Optical transmission was measured after each annealing process at different thicknesses, using a double beam Jasco spectrophotometer UV-VIS-NIR (Model V-670) in the wavelength range of 400-2700nm, a baseline was recorded prior to the actual measurements to calibrate the instrument. Investigations were carried out on the annealed films under the work both separate and together with thickness reduced films.

3. RESULTS AND DISCUSSION

Investigations by XRD using Cu Kα radiation (λ = 1.5406 Å) were carried out to study the structural properties of thin films under the study. X-ray diffraction patterns for the as-prepared layers are shown in Figure. 1. Sharpness of the structural peaks on the diffractograms proves polycrystalline nature of the investigated films. Additionally, the appearance of different peaks on the diffractogram is due to the different orientations of the crystallite structure in the corresponding film sample. Notably, the (015) is the most intense peak indicating the growth favorability of the crystallites in this direction.

It is noteworthy that phases corresponding to all peaks appeared on a certain particular diffractogram were identified using the standard JCPDS data cards of Bi_2Te_3 and Bi_2Se_3 (Cards No. 15-0863 and 33-0214) [9]. The structure is identified in hexagonal form with cell parameters a=4.13960 Å and c=28.63600 Å (space group: R-3m).

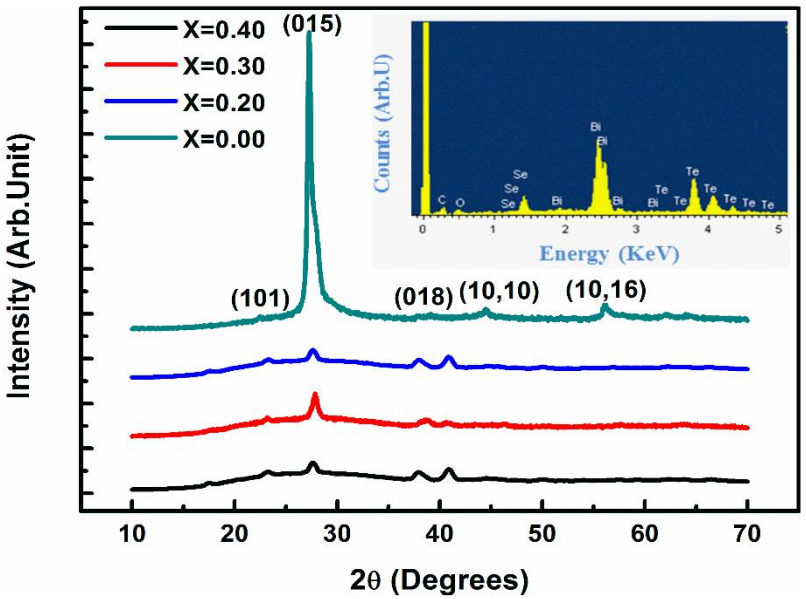

Figure 1 XRD diffraction patterns of as-prepared $Bi_2(Te_{1-x}Se_x)_3$ layers.

The average crystallite size has been calculated by means of the well-known Debye-Scherer's equation:

$$D = \frac{K\lambda}{\beta_{hkl}\cos\theta} \quad (1)$$

Additionally, some important parameters characterizing layer's quality were derived using xrd patterns, Induced strain (Ɛ): $\varepsilon = (\boldsymbol{\beta}_{hkl}.\cos\theta)/4$, dislocation density (d): $d = \frac{1}{D^2}$ and the

number of crystallites per unit area of the film's surface (N): $N = \frac{d}{D^3}$ were calculated using information given by XRD diffraction patterns, values are presented in table 1.

Table 1 structure features of thin $Bi_2(Te_{1-x}Se_x)_3$ layers Inset in Figure 1. Illustrates the elemental. composition analysis of the as prepared $Bi_2Te_{1.8}Se_{1.2}$ thin film (X=0.40), investigated using energy dispersive X-ray analysis (EDAX). Typical stoichiometry of the prepared composition is achieved. In addition, the chemical formula $Bi_2Te_{1.8}Se_{1.2}$ reveals a very nearly bulk material.

Film sample	2θ (degree)	β (radians)	D (nm)	Ɛ	D (cm^{-2})	N (cm^{-2})
0.00	27.279	0.0063	22.5	1.5×10^{-3}	1.9×10^4	17.5×10^4
0.20	27.639	0.018	7.8	4.4×10^{-3}	16×10^4	421×10^4
0.30	27.839	0.0097	14.5	2.3×10^{-3}	4.7×10^4	65×10^4
0.40	27.639	0.019	7.2	4.7×10^{-3}	19.3×10^4	535×10^4

For much deeper study, the surface morphology of the as-prepared films was scanned with the aid of scanning electron microscope (SEM). SEM micrographs are shown in Figure 2. Obviously, all films under the study exhibit homogenous and smooth layer's surface, it can also be seen that substrates are well covered by $Bi_2(Te_{1-x}Se_x)_3$ materials. Additionally, highly crystalline films with extremely small grain size can be observed. It can be concluded from SEM observations that vacuum thermal evaporation technique for Nano-particles based films production is just suitable.

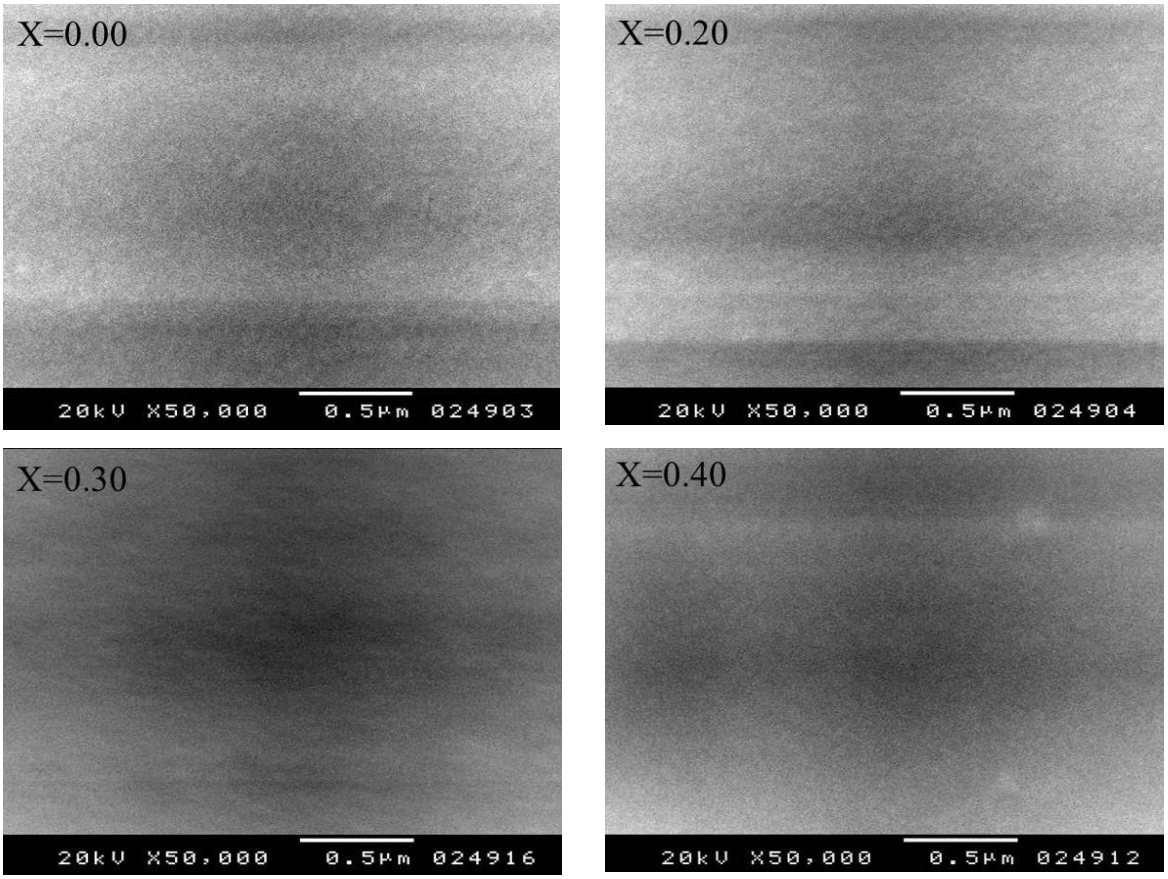

Figure 2 SEM micrographs of as-deposited $Bi_2(Te_{1-x}Se_x)_3$ films.

Optical spectra

As can be seen, optical spectra presented in Figure 3, indicate opaque materials over the whole wavelength range of the study, and in the visible region in particular, as all the light is absorbed at low wavelength (high photon energies). Nevertheless, transmittance showed obvious increase with wavelength increasing, due to low energies of photon (at high wavelength) and consequently no appropriate electronic transitions are possible. In contrast, reflectivity of all films is quite high, as commonly known for semimetals and degenerate semiconductors.

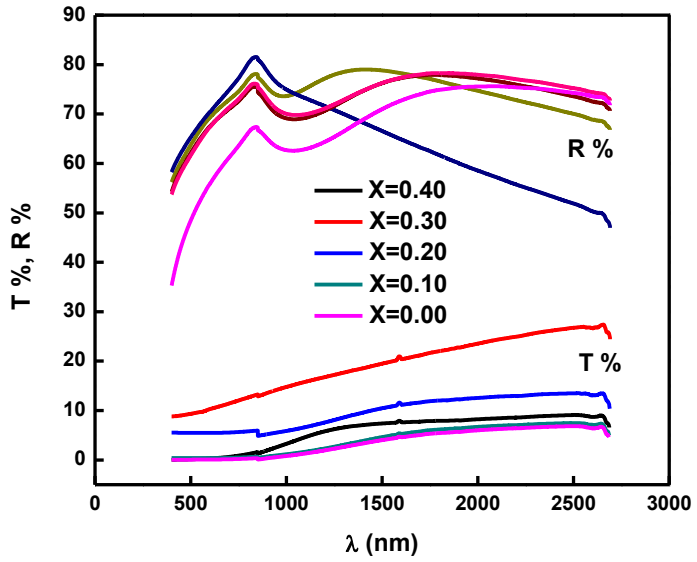

Figure 3 T % and R % of as -prepared Bi_2 $(Te_{1-x}Se_x)_3$ 200 nm thick films

Absorption coefficients (α) was derived from the transmission and reflection measurements, using the approximation formula:

$$\alpha = \frac{1}{d} \mathrm{Ln}\left(\frac{1-R}{T}\right) \quad (2)$$

As indicated in Figure 4, (α) possesses very high values, in the order of 10^7 m^{-1}, in the visible light region, however, a notable decrease is observed as wavelength increased confirming transmittance spectral observations and asserting that Bi_2Te_3-based films have considerable absorption throughout the ultra-violet and visible region [10,11]. In addition, inset shown in Figure 4 indicates the strong compositional dependence of (α). As a general view, Se addition to Bi_2Te_3 enhanced light absorbance which is may be due to the creation of impurity levels in the hosting lattice.

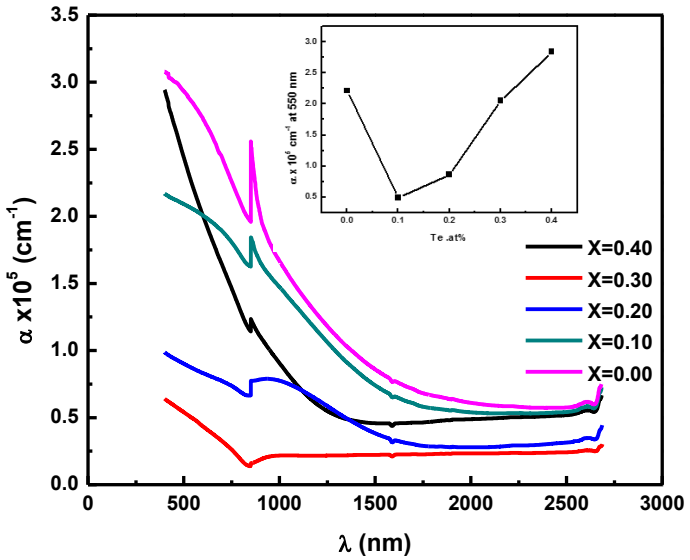

Figure 4 Absorption coefficient of as-prepared Bi_2 $(Te_{1-x}Se_x)_3$ layers at 200 nm.

Band gap energy (E^{Opt}_g) was estimated on the basis of the recorded optical spectra using the following relation [12]:

$$\alpha h\nu = A\,(h\nu - E_g)^n \qquad (3)$$

A is a constant related to band tailing parameter (transition probability), h is Planck's constant and υ is the frequency. In the above equation n=1/2 for a direct allowed transition, n=3/2 for direct forbidden transition, n=2 for an indirect allowed transition and n=3 for indirect forbidden transition [13].

Plots of $(\alpha h\nu)^2$ as a function of photon energy (hν) are shown in Figure 5, n=1/2 used in our case indicating a direct allowed transition in the investigated thin films system. Extrapolating the straight part of $(\alpha h\nu)^2$ versus (hν) relation towards lower energies yields the value of the corresponding forbidden optical energy gap (E^{Opt}_g). The derived (E^{Opt}_g) is expressed in the inset of Figure 5 as a function of Se content. Values of (E^{Opt}_g) are consistent with the previously deduced for the same system [14, 15].

It can be seen in the inset of Figure 5 that E^{Opt}_g increases as much Se is added to Bi_2Te_3 lattice. Such increase can be explained in terms of Moss-Burstein shift effect, which is an effect seen in degenerate semiconductors as a shift with increasing doping of the band-gap as defined as

the separation in energy between the top of the valence band and the unoccupied energy states in the conduction band.

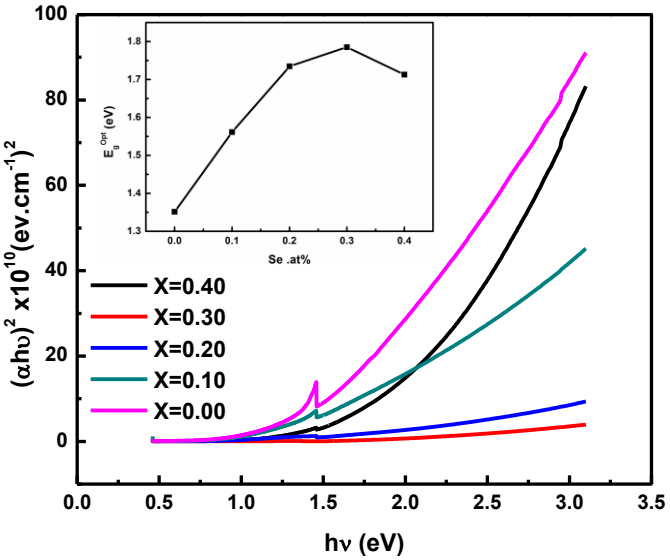

Figure 5 Plots of $(\alpha h\nu)^2$ as a function of photon energy ($h\nu$) of the as-prepared $Bi_2(Te_{1-x}Se_x)_3$ films

Effect of annealing at different thicknesses

The prepared films were annealed for 3h at 250 °C and a simultaneous thickness reduction was done as well. Enhancements in the optical transmittance is expected as a result of annealing and thickness reduction. As a first step to understand the effects of annealing, the structure and surface morphology of the annealed films were studied with the aid of SEM characterizations. Figure 6 illustrates the surface morphology of the annealed films. Intensive observations in the SEM micrographs presented in Figure 6 reveal significant changes in the structure. Notably, grains formed clustered aggregation which is due to enlargement of particle size and lowering of strain and dislocation density [16]. Moreover, crystallinity is enhanced by annealing, that is clearly seen through white spots appeared in the micrographs of the annealed films.

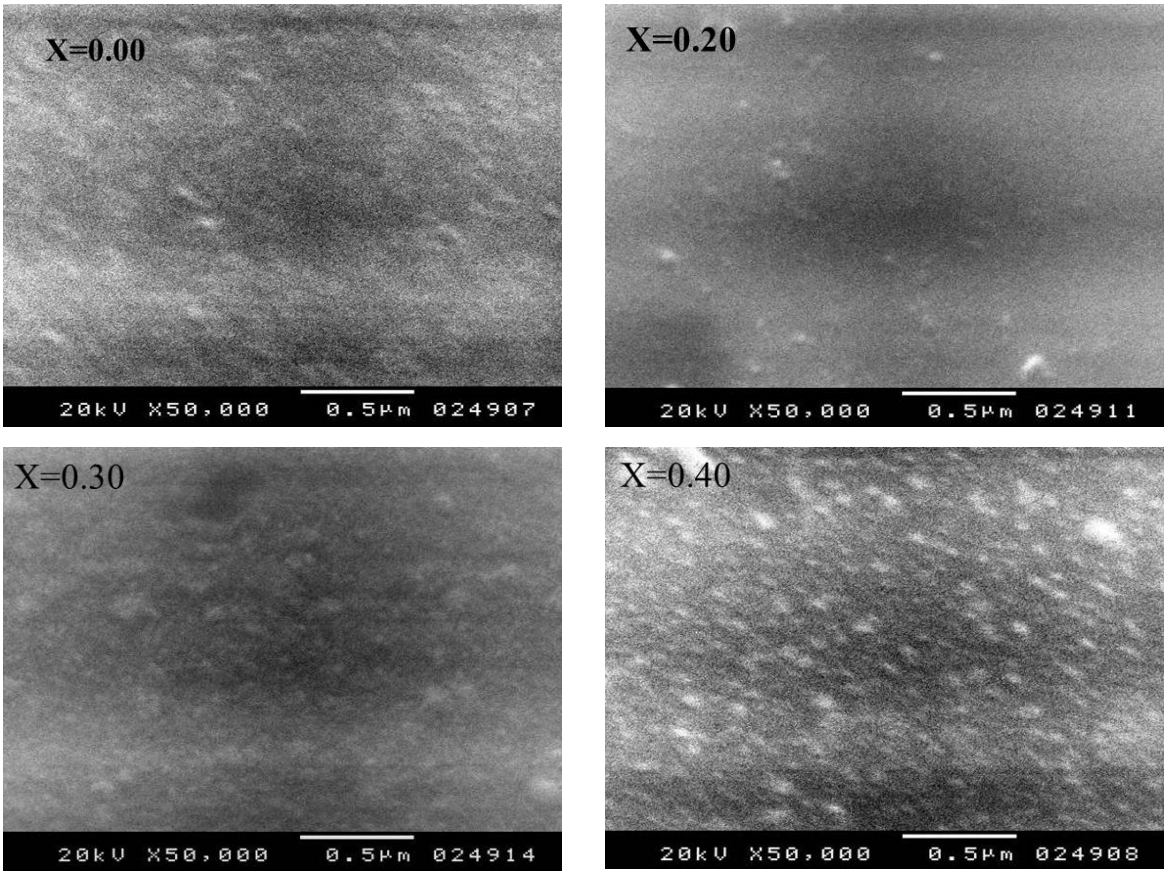

Figure 6 SEM micrographs of annealed thin $Bi_2(Te_{1-x}Se_x)_3$ layers

Optical characteristics of the annealed layers:

Transmittance and reflectance spectra of annealed films with different thicknesses.

Thickness reduction effect

Optical spectra of annealed films at thickness reduced are shown in Figure 7. It is clearly seen that behavior of transmittance and reflectance of the annealed samples are typically the same if compared with that of the as-prepared films. However, a slight decrease in reflection can be noted which is a promising result for enhancing light transmission through the concerned layers.

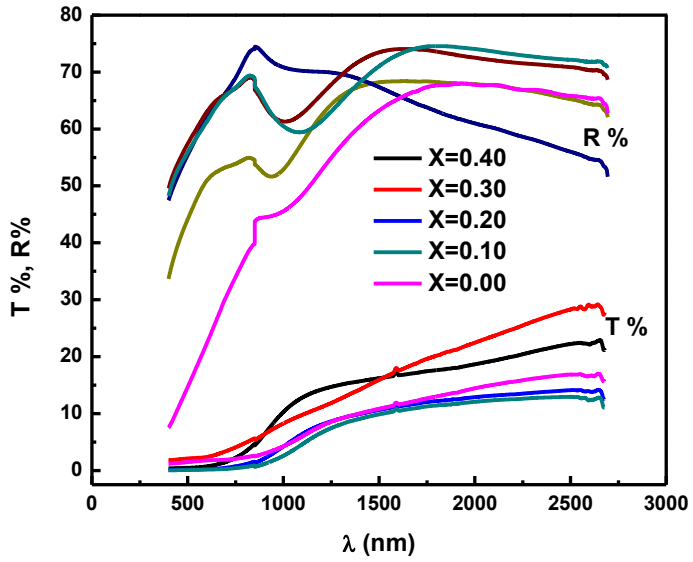

Figure 7 T and R spectra of 100 nm thick $Bi_2(Te_{1-x}Se_x)_3$ films annealed for 3h at 250 °C.

Absorption coefficient (α) is presented for annealed samples in Figure 8 for comparison. It can be said that (α) still has the same behavior and shows almost the same behavior as before annealing.

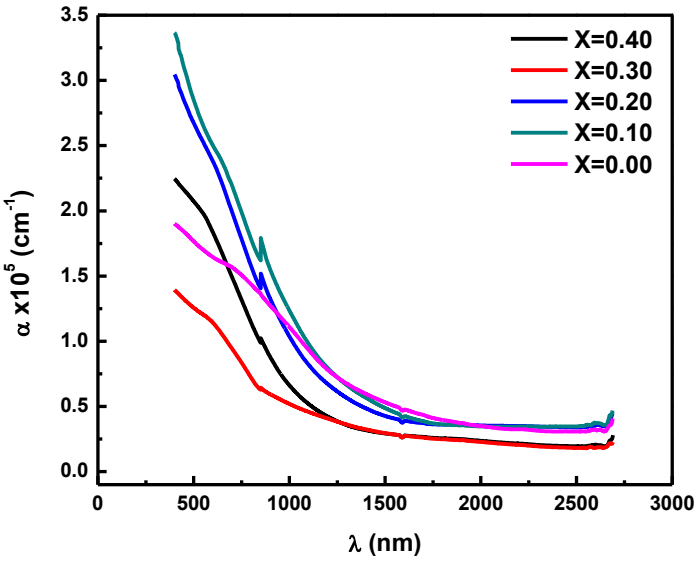

Figure 8 Absorption coefficient of 100 nm thickness layers annealed at 250 °C for 3h

Comparison in terms of absorption reveals that a negligible change in behavior and/or values can be observed, which reflects that the prepared samples exhibit identical structure without defects. Moreover, all changes and enhancements in the transmissivity of the concerned layers

occurred at the expense of reflectivity as can be seen from transmittance and reflectance spectra.

Optical energy gap E^{Opt}_g is calculated using the same method, Figure 9 shows photon energy dependence of $(\alpha h\nu)^2$ of 100 nm thickness layers annealed at 250 °C for 3h. as illustrated in the figureure inset, E^{Opt}_g decreased significantly due to annealing, which is attributed to enhancements in the crystal structure of the annealed films. Furthermore, inset of Figure 9 depicts the compositional dependence of E^{Opt}_g, it is clear again that Se doping enlarges the energy band gap.

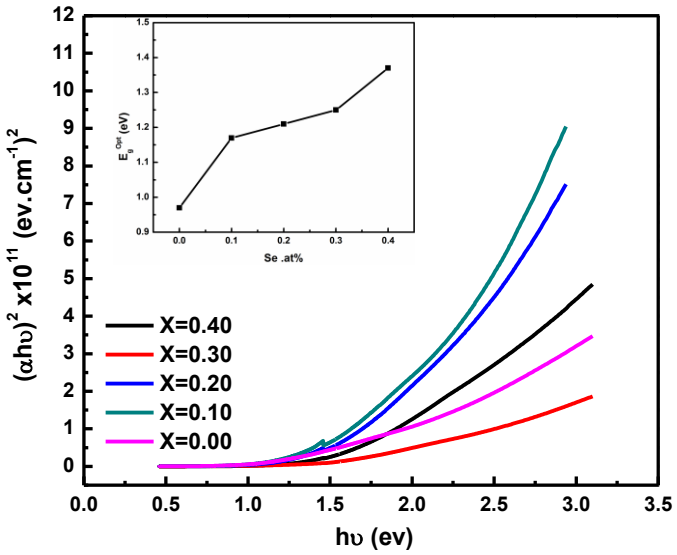

Figure 9 Absorbance plots of 100 nm-thick layers annealed at 250 °C for 3h

In the next section, we will discover the effect of thickness reduction on the optical transmissivity in the concerned layers. Figure 10 shows transmissivity and reflectivity of 35 nm films. A significant increase in transmission is clearly seen. At Se doping of 30% the transmissivity reached 60%, i.e. 3 times higher than the transmissivity in 200 and 100 nm thickness layers shown in Figure 3 and Figure 7. The few-layer Bi_2Te_3-Bi_2Se_3 can significantly enlarge the surface-to-volume ratio, and can be considered as a ‘‘quantum dot’’ that would result in quantum confinement [17].

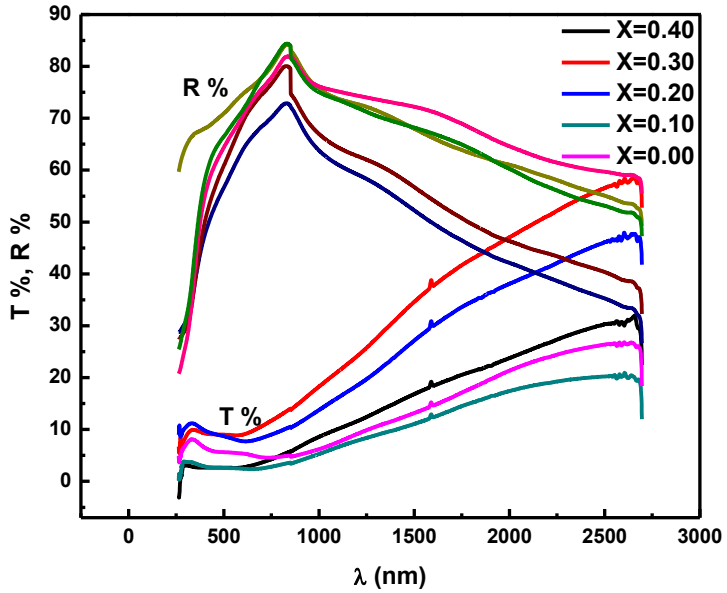

Figure 10 T and R spectra of 35 nm thick $Bi_2(Te_{1-x}Se_x)_3$ films annealed for 3h at 250 °C

Remarkably, absorption coefficient (α) seems to follow three steps decreasing behavior against wavelength increasing. However, the presented values of (α) in Figure 11 are almost in the same range of the previously given in Figure 4 and Figure 8.

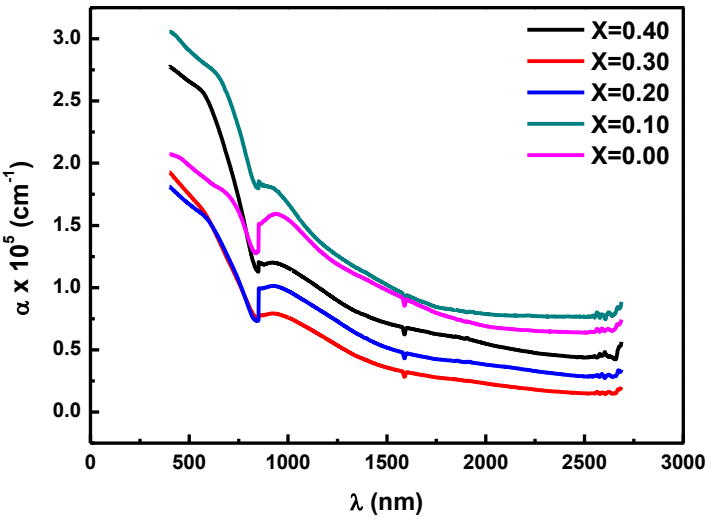

Figure 11 Absorption coefficient of 35 nm thickness layers annealed at 250 °C for 3h

On the other hand, absorption coefficient calculations were employed according to Tauc equation to derive the optical band gap of the investigated layers, as before. Inst of Figure 12 illustrates variation of optical band gap E^{Opt}_g with Se amounts in each sample. It can be seen

that E^{Opt}_g shows an opposite behavior to the behavior presented in Figure 5 and Figure 9. Moreover, E^{Opt}_g appeared in much smaller values and showed a decreasing trend, which confirms the structure enhancements occurred due to simultaneous annealing and thickness reduction. Additionally, the concentration of localized states in the band structure gradually increases due to annealing treatment, hence an increase in the energy width of localized states occurred in the annealed films, and thereby the optical band gap was notably reduced [18]. The few-layer nanomaterials would possess excellent performance in saturable absorption, and could be a potentially saturable absorber. Therefore, a strong motivation was shown in [17] to develop the pulsed fiber lasers Q-switched with few-layer Bi_2Se_3 as the saturable absorber.

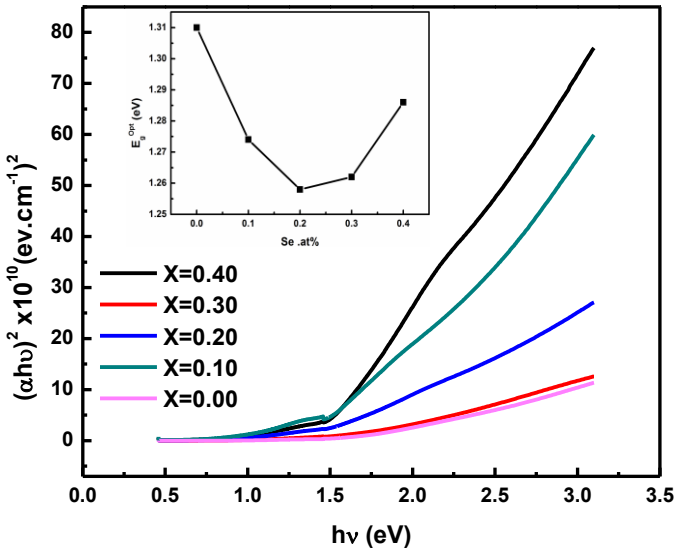

Figure 12 Absorbance plots of 35 nm-thick layers annealed at 250 °C for 3h.

Further decreasing in thickness led to significant increasing in transmissivity as one can see in Figure 13. 15 nm thick layers showed maximum transmittance of 96.4% at wavelength of 2600 nm.

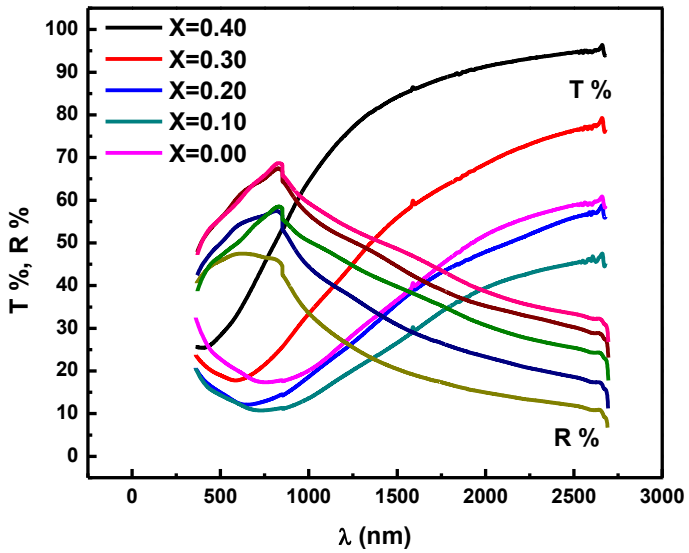

Figure 13 T and R spectra of 15 nm thick $Bi_2(Te_{1-x}Se_x)_3$ films annealed for 3h at 250 °C.

It can be clearly noted that the thickness decreasing led to a significant increase in the materials transmittance. As the as-prepared films (200 nm) showed maximum transmittance lower than 30 % which appeared at higher wavelength, whilst, the miniaturized films (15 nm) exhibited transmissivity of up to 96.4 %. On the other hand, reflection decreased seriously.

In general, and at different thicknesses, behavior of transmissivity and reflectivity still unchanged, the seen behavior can be explained in terms of light absorbance in the concerned materials. As one can be notice, a remarkable change in values and behavior of absorption coefficient (α) is depicted in Figure 14.

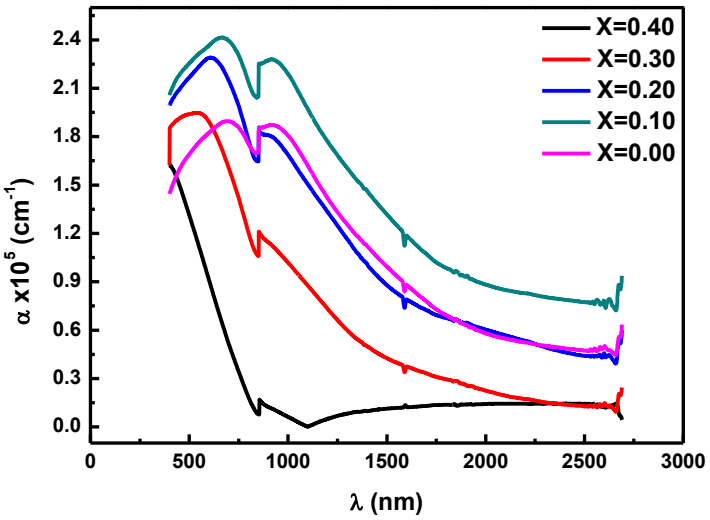

Figure 14 Absorption coefficient of 15 nm thickness layers annealed at 250 °C for 3h.

The concerned few-layer of the Se doped Bi_2Te_3 demonstrate an interesting absorption in the visible light region, as the absorption spectrum of few-layer system depends on the size and number of layers. Plots of αhν as a function of photon energy (hν) are shown in Figure 15 for 15 nm thick layers annealed at 250 °C for 3h, in our case, plots of αhν versus (hν) indicate a direct allowed transition in the prepared layers.

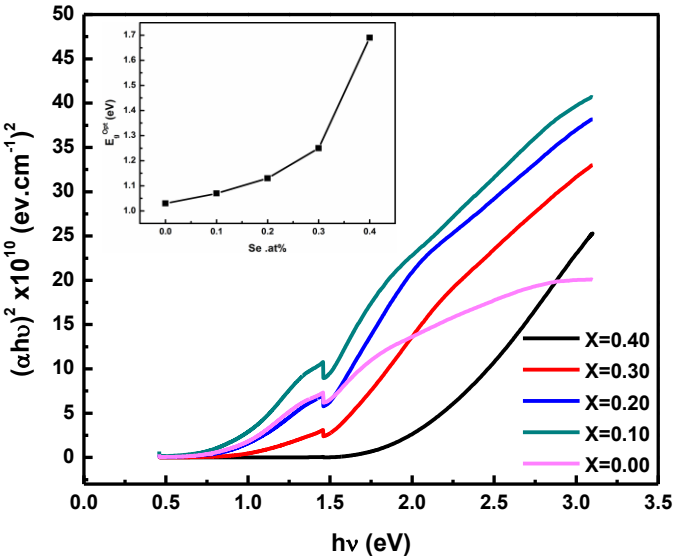

Figure 15 Absorbance plots of 15 nm-thick layers annealed at 250 °C for 3h

The reason for this larger Eg of few-layer system under the study is due to the well-known quantum confinement effect by shifting the conduction and valence band edges in opposite directions [19-21]. It is worth mentioning that, for a 2D crystallite, the band gap shift, DE_g, is described by the equation [22,23]:

$$\Delta E_g = \frac{h^2}{4\mu_{xy}L_{xy}^2} + \frac{h^2}{8\mu_z L_z^2} \quad (4)$$

where μ_{xy} and μ_z are the reduced effective masses of electron-hole pairs in parallel (xy) and perpendicular (z) directions, respectively, and L_{xy} and L_z are the corresponding dimensions of the crystallite. To summarize, a comparative analysis for transmittance (T) at different thicknesses is shown in the table below. It is clear that T increased profoundly due to thickness reduction.

Table 2 Comparative study of transmittance enhancement in different thickness layers for samples annealed at 250 °C, at wavelength of 2600 nm.

Layer's sample	As-prepared	T % of 100 nm	T % of 35 nm	T % of 15 nm
X=0.40	8.7	22.1	30.2	96.4
X=0.30	26.7	29.1	57.9	76.7
X=0.20	13.1	14.0	47.7	56.5
X=0.10	7.1	12.4	20.5	45.9
X=0.00	6.4	16.6	26.7	59.0

References

[1] A.Y. Morsy, S.S. Fouad, E. Hashem and A.A. EL-Shazly, ACTA PHYSICA POLONICA A, 80 (1991) 819
[2] J. Dheepa, R. Sathyamoorthy, A. Subbarayan, Journal of Crystal Growth, (2005), 274, 100
[3] V. Damorada Das, P. Gopal Ganesan, Semicond. Sci. Technol. 12 (1997) 195
[4] S. Golia, M. Arora, R.K. Sharma, A.C. Rastogi, Curr. Appl. Phys. 3 (2003) 195
[5] N.G. Patel, P.G. Patel, Solid State Electron. 35 (1992) 1269
[6] S.A. Omer, U.G. Isifield, Solar Energy Mater. Solar Cell. 53 (1998) 67
[7] J.C. Tedenac, S. Charar, Phys. Low Dimens. Struct. 5/6 (2000) 61
[8] H.E.A. El-Sayed, Applied Surface Science 250 (2005) 70
[9] A. Kadhim, A. Hmood, H. Abu Hassan, Materials Letters 65 (2011) 3105
[10] J. Dheepa, R. Sathyamoorthy, S. Velumani, Materials Characterization, 58 (2007) 782
[11] G. D. Deshmukh, S. M. Patil, S. S. Patil, and P. H. Pawar, JCBPS; Section C 5 (2015) 2769

[12] G. Saffarini, J.M. Saiter, H. Schmitt, Opt. Mater. 29 (2007) 1143
[13] J. Tauc, Amorphous and Liquid Semiconductors, Plenum, New York, (1979)
[14] V. M. Garcıa, M. T. S. Nair, P. K. Nair, and R. A. Zingaro, Semiconductor Science and Technology 12 (1997) 645
[15] Saji Augustine, Ampili S., Jeung Ku Kang and Elizabeth Mathai., Materials Research Bulletin 5 (2005) 1314
[16] Shailaja Jeetendra, Naveen C. Shivappa, Raghu Patel, Mahesh H. Matt, "Optimization of Thickness of Sb_2Te_3 Thin Film as Back Contact for CdTe Thin Film Solar Cells", DOI: 10.5185/amlett.2014.7589, in press.
[17] Liping Sun, Zhiqin Lin, Jian Peng, Jian Weng, Yizhong Huang, Zhengqian Luo, SCIENTIFIC REPORTS 4 (2014) 1
[18] Farid M. Abdel-Rahim, M.M. Hafiz, H. Alsorory, Journal of Alloys and Compounds 570 (2013) 76
[19] Brus, L. A simple model for the ionization potential, electron affinity, and aqueous redox potentials of small semiconductor crystallites. J. Chem. Phys. 79 (1983) 5566
[20] Henglein, A. Small-particle research: physicochemical properties of extremely small colloidal metal and semiconductor particles. Chem. Rev. 89 (1989) 1861
[21] M. Mourad Mabrook, Exp. Theo. NANOTECHNOLOGY 2 (2018) 103
[22] Sandroff, C., Hwang, D. & Chung,W. Carrier confinement and special crystallite dimensions in layered semiconductor colloids. Phys. Rev. B 33 (1986) 5953
[23] Smotkin, E. et al. Size quantization effects in cadmium sulfide layers formed by a Langmuir-Blodgett technique. Chem. Phys. Lett. 152 (1988) 265